EVALUATION OF A SIMPLIFIED HIGH FREQUENCY INJECTION POSITION SENSORLESS CONTROL METHOD FOR RELUCTANCE SYNCHRONOUS MACHINE DRIVES

W.T. Villet*, M.J.Kamper*, P. Landsmann**, and R. Kennel**

*Electric Machines Laboratory
University of Stellenbosch, Stellenbosch, South Africa
e-mail: 15053830@sun.ac.za, kamper@sun.ac.za

** Institute for Electrical Drive Systems and Power Electronics
Technische Universitaet Muenchen, Munich, Germany
e-mail: peter.landsmann@tum.de

Keywords: Alternating High Frequency Injection, Sensorless Control, Reluctance Synchronous Machines

Abstract

In this paper a simplified and stable high frequency injection sensorless control method for reluctance synchronous machine drives is presented. This method is based on previous work where the conventional band pass filter is omitted from the demodulation scheme to prevent unnecessary time delay and magnitude decrease. Previous work presented accurate position estimation at very low speed under no-load conditions. The proposed method is evaluated under various different load conditions and at high speeds. The performance of the proposed method is compared to the performance of the drive while using a rotary encoder. Experimental results show that the scheme is stable under various load conditions and delivers good performance.

1 Introduction

Position sensors for electrical machines are expensive and reduce the reliability of the drive, not only because of the sensor itself, but also because of the link between the sensor and the controller. The high frequency (HF) injection sensorless method has received a lot of attention throughout the years and has become a popular choice for synchronous machines, due to its ability to estimate the rotor position at standstill.

Conventional HF injection methods as explained and used by [7], [9] and [10] amongst others, make use of a band pass filter in the demodulation scheme, followed by a low pass filter. Investigations by [11] show the possibility of a simplified demodulation scheme by omitting the conventional band pass filter. Filters can have a negative effect on machine control. In some cases filters can also cause unnecessary magnitude decrease of the measured signal. Digital implementation of filters causes time delay.

In [11] the estimation capabilities of the scheme are analysed with and without the band pass filter on a PMSM drive. Measured results at 1.5 rpm at no load showed very good position estimation. However the performance of this method at higher speeds and under load conditions is thus still unknown. These aspects are investigated on a reluctance synchronous machine (RSM) drive. The RSM is known to be robust and comparably efficient under correct control algorithms [3]. Another aspect that receives attention in this paper is the dynamic performance of the simplified method.

2 HF carrier injection method

In this method a high frequency voltage vector is superimposed onto the fundamental control voltage vector in the estimated anisotropy reference frame. An amplitude modulation scheme is used to track the saliency induced by saturation along the axis orthogonal to the injection axis [9]. This enables the demodulation scheme to track the anisotropy position of the rotor [7]. The anisotropy in a reluctance machine rotates at the same angular frequency as the rotor.

2.1 High Frequency Machine Model

The RSM can be modelled in the synchronous rotor reference frame (dq) as in Equation (1), where $\mathbf{u}_s^{(r)} = \begin{bmatrix} u_{Sd} \\ u_{Sq} \end{bmatrix}$ is the stator voltage, $\mathbf{i}_s^{(r)} = \begin{bmatrix} i_{Sd} \\ i_{Sq} \end{bmatrix}$ the stator current and R_s the stator resistance. The angular speed of the synchronous reference frame is represented by ω. Superscript r denotes quantities in the rotor fixed synchronous reference frame (dq).

$$\mathbf{u}_s^{(r)} = R_s \mathbf{i}_s^{(r)} + \mathbf{L}^{(r)} \frac{d\mathbf{i}_s^{(r)}}{dt} - \omega \mathbf{J} \mathbf{L}^{(r)} \mathbf{i}_s^{(r)} \tag{1}$$

J is an orthogonal rotation matrix and **T** is a transformation matrix used to transform vectors from one reference frame to another.

$$\mathbf{J} = \mathbf{T}(\frac{\pi}{2}) = \begin{bmatrix} 0 & -1 \\ 1 & 0 \end{bmatrix} \tag{2}$$

$$\mathbf{T} = \begin{bmatrix} cos(\theta) & -sin(\theta) \\ sin(\theta) & cos(\theta) \end{bmatrix} \quad (3)$$

$$\mathbf{T}^{-1} = \begin{bmatrix} cos(\theta) & sin(\theta) \\ -sin(\theta) & cos(\theta) \end{bmatrix} \quad (4)$$

The inductance vector, $\mathbf{L}^{(r)}$ as used by [4] is described by:

$$\mathbf{L}^{(r)} = \begin{bmatrix} L_d & 0 \\ 0 & L_q \end{bmatrix} \quad (5)$$

Evaluating Equation (1) at high frequencies that are bounded as by Equation (6), where f_s is the sampling frequency and ω_r is the maximum operating fundamental frequency, the resistive- and speed voltage terms fall away due to its small magnitudes compared to the inductance term [4]. Equation (1) simplifies to (7) where subscript c refers to the carrier frequency component of each quantity. The model of the RSM under high frequency carrier-signal excitation is a pure inductive load [9].

$$2\omega_r < \omega_{HF} < \frac{2\pi f_s - 2\omega_r}{2} \quad (6)$$

$$\mathbf{u}_{sc}^{(r)} = \mathbf{L}^{(r)} \frac{d\mathbf{i}_{sc}^{(r)}}{dt} \quad (7)$$

2.2 Alternating Carrier Injection

An alternating carrier voltage is applied to the estimated real axis (d-axis) in the dq- reference frame at a constant carrier frequency ω_c [1] [4]. The vector is kept in alignment with the observed d-axis which is real [7]. Figure 1 shows the discrete Fourier transform of the injection voltage, $u_c cos(\omega_c t)$ at 3 kHz with a sampling frequency of 10 kHz. The frequency spectrum of the applied voltage, $u_d + u_c cos(\omega_c t)$, is shown in Figure 2. It is clear that the injection voltage is significantly smaller than the applied voltage.

The injected carrier voltage (8) is always transformed to the stationary reference frame by using the estimated electrical position, $\hat{\theta}_e$ [7]. Equation (8) is in the stationary ($\alpha\beta$) reference frame as indicated by superscript (s). Estimated values are represented with a hat.

$$u_{sc}^{(s)} = u_c cos(\omega_c t) e^{j\hat{\theta}_e} \quad (8)$$

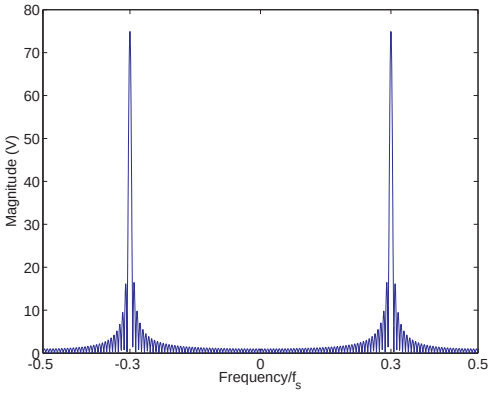

Figure 1: DFT of HF injection voltage

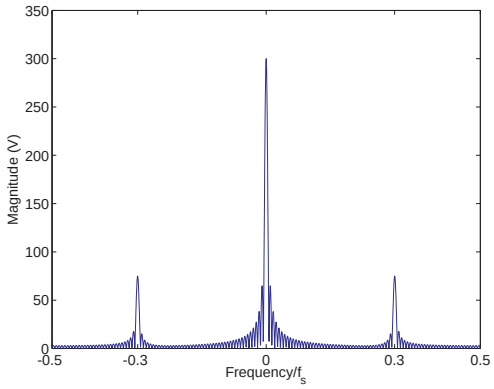

Figure 2: DFT of applied voltage

Usually stator current measurements are used as feedback, thus the measured current is used to calculate the actual anisotropy position. Equation (7) can be rewritten as in (9). Equation (9) is the current response in the actual dq reference frame. The current can only be measured in the estimated dq reference frame given by Equation (10) [4]. The current in the rotor reference frame is transformed to the stationary reference frame by the actual rotor position. This is the current that is measured.

$$\mathbf{i}_{sc}^{(r)} = \mathbf{L}^{(r)^{-1}} \int \mathbf{u}_{sc}^{(r)} dt \quad (9)$$

$$\mathbf{i}_{sc}^{(\hat{r})} = \mathbf{i}_{sc}^{(s)} e^{-j\hat{\theta}_e} = \mathbf{i}_{sc}^{(r)} e^{j(\theta_e - \hat{\theta}_e)} \quad (10)$$

$$= \frac{u_c \mathbf{L}^{(r)^{-1}}}{\omega_c} sin(\omega_c t) e^{j(\theta_e - \hat{\theta}_e)} \quad (11)$$

The estimation error can be represented by $\Delta\theta_e = \theta_e - \hat{\theta}_e$. If $\Delta\theta_e$ is small enough and if the closed loop system is in steady state i.e. the estimated angle tracks the actual angle, it is a reasonable assumption that $e^{-j\Delta\theta_e}$ is nearly time invariant. If $e^{-j\Delta\theta_e}$ is indeed almost time invariant it will not result in a frequency shift and thus only scale the frequency components. This assumption can lead to simplifications of $sin(\Delta\theta_e) \approx \Delta\theta_e$ and $cos(\Delta\theta_e) \approx 1$. It is necessary to transform Equation (5) to the estimated rotor frame using Equations (12) and (13).

$$\mathbf{L}_s^{(\hat{r})} = \mathbf{T}\mathbf{L}_s^{(r)}\mathbf{T}^{-1} \quad (12)$$

$$\mathbf{T} = \begin{bmatrix} cos(\Delta\theta_e) & -sin(\Delta\theta_e) \\ sin(\Delta\theta_e) & cos(\Delta\theta_e) \end{bmatrix} \quad (13)$$

Simplification of the mathematics leads to:

$$\mathbf{L}^{(\hat{r})} = L_m \mathbf{I} + \Delta L \begin{bmatrix} cos(2\Delta\theta_e) & sin(2\Delta\theta_e) \\ sin(2\Delta\theta_e) & -cos(2\Delta\theta_e) \end{bmatrix} \quad (14)$$

where $L_m = (L_d + L_q)/2$ is the mean position independent inductance and $\Delta L = (L_d - L_q)/2$ describes the magnitude of the saliency [4] [6]. $\mathbf{I}$ is the 2x2 identity matrix. The inverse of Equation (14) is derived in Equation (15) [4]. Substituting Equation (15) into Equation (11) and applying assumptions as noted above the current in the observed synchronous rotating reference frame is derived as in Equation (16) [4] [6].

$$\mathbf{L}^{(\hat{r})-1} = \frac{1}{L_d L_q}\Big[L_m\mathbf{I} + \Delta L \begin{bmatrix} -cos(2\Delta\theta_e) & -sin(2\Delta\theta_e) \\ -sin(2\Delta\theta_e) & cos(2\Delta\theta_e) \end{bmatrix}\Big] \quad (15)$$

$$\mathbf{i}_{sc}^{(\hat{r})} = \frac{u_c sin(\omega_c t)}{L_d L_q \omega_c}\Big[L_m \begin{bmatrix} 1 \\ 0 \end{bmatrix} - \Delta L \begin{bmatrix} cos(2\Delta\theta_e) \\ sin(2\Delta\theta_e) \end{bmatrix}\Big] \quad (16)$$

It is now clear that the second term on the right contains information regarding the position estimation error and is strongly dependent on the magnitude of the saliency.

2.3 Sensorless Control Approach

The symmetrical spectrum in Figure 2 suggests that the pulsating vector can be interpreted as superposition of two rotating vector carriers [9]. The carrier signal appears to lack spectral separation which is essential for synchronous reference frame filtering [9].

According to [8], the spectrum of signal $x(t)$ is shifted to the carrier frequency when multiplied by $cos(\omega_c t)$, as in Equation (17).

$$x(t)cos(\omega_c t) \Longleftrightarrow \frac{1}{2}[X(\omega+\omega_c) + X(\omega-\omega_c)] \quad (17)$$

Multiplying the measured current in Equation (16) with $sin(\omega_c t)$ leads to the derivation of the trigonometry identity of Equation (18).

$$sin^2(\omega_c t) = \frac{1 - cos(2\omega_c t)}{2} \quad (18)$$

When evaluating Equation (18) in the frequency domain it is clear that there is one component at the origin and two components at twice the carrier frequency. The effect of the frequency shift (unscaled with respect to parameters) can be seen in Figure 3.

The component at the origin can be used to extract the rotor position. It is now clear that a simple low pass filter can separate this component from the other high frequency components.

This transformation generates a high frequency current signal that is easy to demodulate without referring to machine parameters [7]. Assuming that the remaining high frequency current components are rejected by a low pass filter after applying the trigonometry identity of Equation (18) the low pass filtered current is described by Equation (19).

$$\mathbf{i}_{LPF}^{(\hat{r})} = \frac{u_c}{2L_d L_q \omega_c}\Big[L_m \begin{bmatrix} 1 \\ 0 \end{bmatrix} - \Delta L \begin{bmatrix} cos(2\Delta\theta_e) \\ sin(2\Delta\theta_e) \end{bmatrix}\Big] \quad (19)$$

Further simplifications as discussed earlier lead to:

$$\mathbf{i}_{LPF}^{(\hat{r})} = \frac{u_c}{2L_d L_q \omega_c}\Big[L_m \begin{bmatrix} 1 \\ 0 \end{bmatrix} - \Delta L \begin{bmatrix} 1 \\ 2\Delta\theta_e \end{bmatrix}\Big] \quad (20)$$

Equation (20) indicates that the q-axis current component in the estimated rotor reference frame becomes zero when the rotor position angle error is zero [2]. Thus only the q-axis component could be processed to acquire the rotor position [2]. It is important to observe that the information of the rotor position strongly depends on the magnitude of the saliency ΔL [2]. The error signal will disappear when $L_d = L_q$ [2].

2.4 Demodulation of Position Estimation Error

Equation (20) shows that the q-component of the current response is proportional to the estimation error $\Delta\theta_e$. This is used to track the electrical angle in a phase locked loop (PLL) system [7]. The PLL relies on the fact that proper frame orientation results in the carrier current component decoupling such that current only exists in the excited d-axis [9]. The estimator is in effect an amplitude null regulator [9].

Tracking an error signal is robust against noise and measurement tolerances e.g. the limited resolution of analog to digital converters in drive controllers [7]. The proposed scheme for sensorless position detection is shown in Figure 4.

As seen in this scheme it is proposed that only a low pass filter be used in the demodulation scheme. Conventional HF injection schemes make use of an extra band pass filter before multiplying i_q with $sin(\omega_c t)$. As proven above it is not necessary to use a band pass filter. The design of the band pass filter is critical to ensure that only the components around the carrier frequency are filtered out. This requires a sharp roll-off frequency. However sharp roll-off causes the problem of phase shift.

Additional to the phase shift, filters also cause magnitude decrease. Filters implementation in ANSI-C causes a time delay.

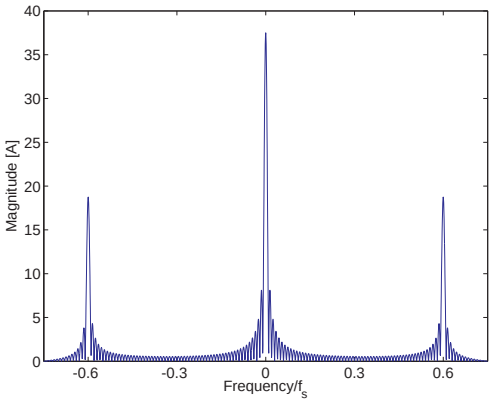

Figure 3: Frequency shifted current

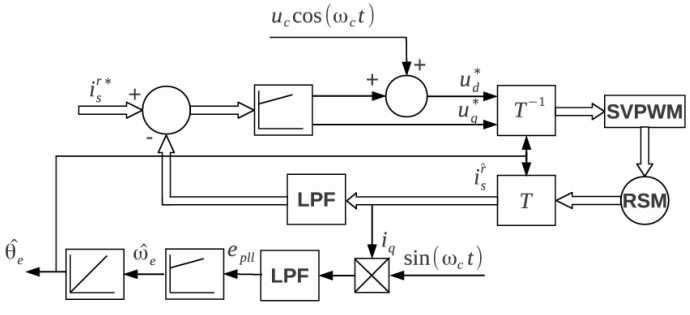

Figure 4: Block diagram of alternating HF injection sensorless control

Filter also change the dynamic response of the whole system and therefore impair the PLL tuning capabilities. The implementation of the low pass filter is done with a simple first order filter. First order filters are easy to implement and configure.

3 Measured Results

The specifications of the RSM used are listed in Table 1. The test bench is shown in Figure 5. The RSM (orange) is coupled to an induction machine (IM)(blue) that acts as a load. Each machine is driven by a $5\ kW$ inverter with the DC links bridged. The inverters are controlled by a LINUX based real time application interface.

Pole pairs	2	
Nominal power	1.1	kW
Rated current	3.5	A RMS
Rated mechanical torque	7	Nm
Rated mechanical speed	157	rad/s

Table 1: RSM specifications

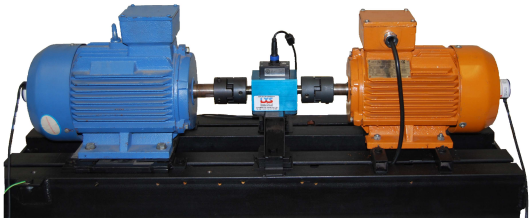

Figure 5: Test bench used with the IM on the left and the RSM on the right

As discussed earlier, the error signal is strongly dependent on ΔL, thus it is necessary to have a difference in inductances for the tracking scheme to work. The measured flux and inductance in the dq reference frame are displayed in Figure 6, highlighting the non-linearity of the RSM.

It is necessary to saturate ψ_q to achieve a difference in inductance. To saturate ψ_q, there should always be a small current in the q-axis. To ensure that the difference in inductance is always big enough to track the saliency, i_q was always kept at a minimum of $1.5\ A$. This allows the scheme to track the saliency position from standstill up to base speed and beyond.

3.1 No Load Speed Response

As expected from a HF injection scheme, it is possible to achieve speeds much higher than base speed at no load using the proposed method. Figure 7 shows the estimated electrical position and the measured electrical position at a speed of 0.133 $p.u$ as well as the estimation error. The estimation error seems to oscillate around 2.5^o.

To investigate the dynamic performance of the speed controller, the peak overshoot (M_p) as well as the 2% settling time are examined and compared to a scheme that makes use of a rotary encoder. The results of a series of no load speed response tests

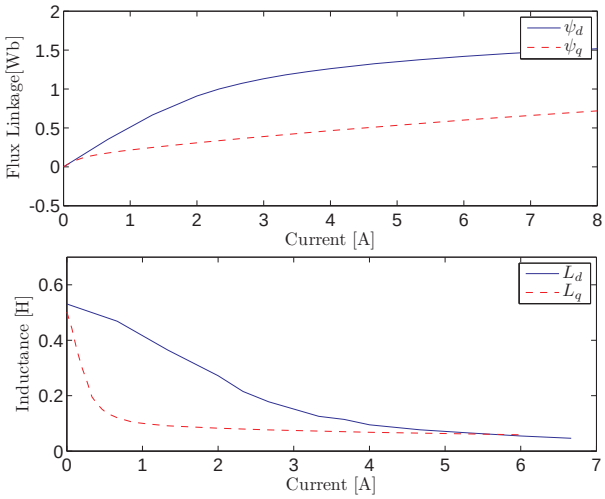

Figure 6: Non-linear characteristics of the RSM

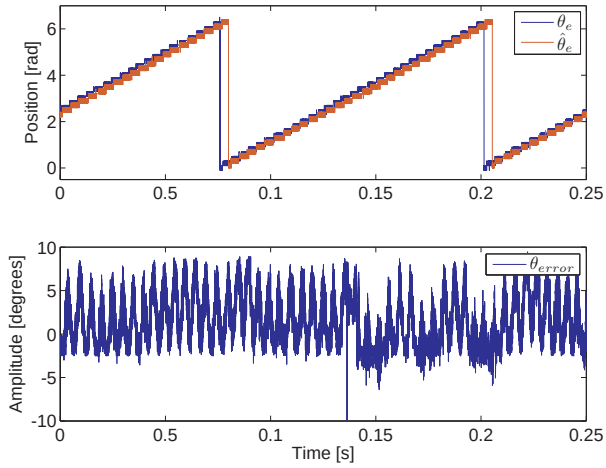

Figure 7: Electrical position estimation and accompanied error at a speed of 0.133 $p.u$

are summarised in Table 2. These tests are performed by applying a reference speed at standstill. Figure 8 shows the results of the 0.933 p.u test.

To further test the dynamics and robustness of the sensorless method a series of tests is performed where a reference speed is applied to the RSM. The direction of the reference speed is then reversed forcing the machine to change direction and acquire the same speed in the opposite direction. The results of these tests are shown in Table 3. These tests highlight the dynamic capability of this scheme especially during direction change.

	Normal Operation		Sensorless Control	
ω_r [p.u]	Mp	2% Settling Time	Mp	2% Settling Time
0.133	0	0.060 s	24	0.495 s
0.667	0	0.058 s	10	0.507 s
0.933	0	0.2075 s	7.14	0.528 s
1.33	0	0.307 s	-1.5	0.560 s

Table 2: Speed response under no load

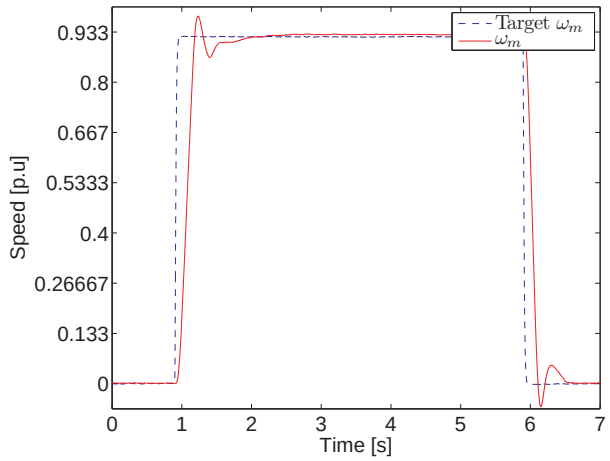

Figure 8: No Load Speed Response

	Normal Operation		Sensorless Control	
ω_r [p.u]	Mp	2% Settling Time	Mp	2% Settling Time
0.133	0	0.090 s	-28	1.021 s
0.4	0	0.151 s	-5	0.66 s
0.667	0	0.251 s	-6	0.829 s
0.933	0	0.359 s	-4.28	0.816 s
1.0667	0	0.390 s	-2.5	0.969 s
1.2	0	0.460 s	-2.22	0.801 s
1.33	0	0.510 s	-2	1.035 s

Table 3: Dynamic response under no load

3.2 Speed response under load conditions

It is clear that the injected high frequency voltage uses a large percentage of the DC bus voltage. This can be problematic under load conditions or during rotor direction change, as the DC bus voltage can vary under these conditions. It is thus necessary to keep the injection voltage as small as possible, but large enough to extract the position. In this project the applied voltage is kept to a minimum of 37% of the maximum limit.

If the maximum DC link voltage is reached, an anti-integration windup function limits the voltage by stopping the integration of the current controller. Unfortunately the addition of a cascade controller for speed control limits the startup torque under speed control to 0.6 p.u torque.

Using 37% of the DC bus voltage for high frequency injection voltage, it is possible to achieve 0.6 p.u torque at rated speed with speed control. Again a series of speed tests are performed as shown in Table 4.

	Normal Operation		Sensorless Control	
ω_r [p.u]	Mp	2% Settling Time	Mp	2% Settling Time
0.133	0	0.145 s	0	1.33 s
0.4	0	0.380 s	3.33	2.363 s
0.67	0	0.867 s	0	2.587 s
0.8	0	1.286 s	0	1.6 s
0.93	0	1.777 s	0	1.6754 s

Table 4: Speed response at 0.6 p.u torque

The speed response and the accompanied estimation error are investigated by applying and removing a load at constant speed as shown in Figure 9. The estimation error increases oscillating around -10^o. This is to be expected under high load conditions. During measurements of [9], the estimation error oscillated around -25^o under similar load conditions.

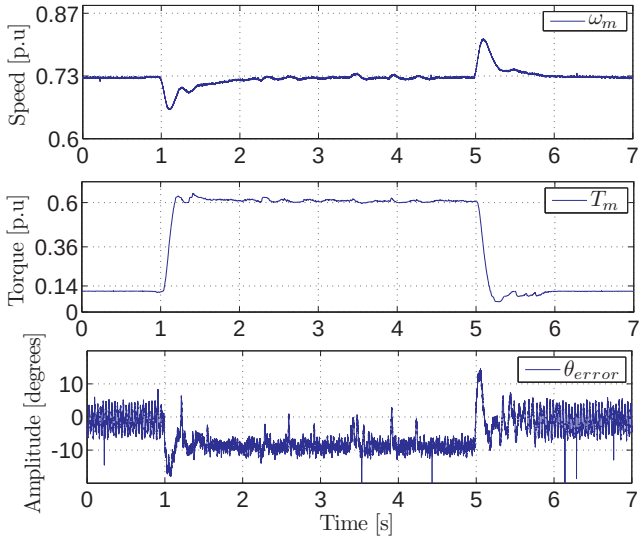

Figure 9: Speed Response to applied load

3.3 Torque control

Operating in torque control the sensorless method performs well and is able to deliver above rated torque from standstill up to base speed. In Figure 10 the RSM applies a load of 1 $p.u$ to the IM. The 2% settling of the current vector is 32 ms.

4 Limits of stable operation

The speed-torque stability of the proposed scheme is investigated in torque control while being driven at set speeds by the IM. The resultant stable area of operation is shown in Fig. 11. These results indicate at what load conditions the method will lose track of the rotor position.

The thick solid line indicates the proposed method and the dotted line the curve fitted line of this method. The method is compared to a method used by [5]. As shown in Figure 6 the saliency (ΔL) disappears at low- and high loads which can cause the estimation method to lose track of the rotor position. It is clear that the scheme presented in this paper is not able to produce as high startup torque as that of [5], but it is able to produce higher torque in the mid speed range up past base speed. The startup torque is still high at 1.86 p.u.

Figure 11 proves that despite very high torque, the proposed method is able to track the rotor position in the entire speed region of the drive and even beyond the rated speed while operating in torque control.

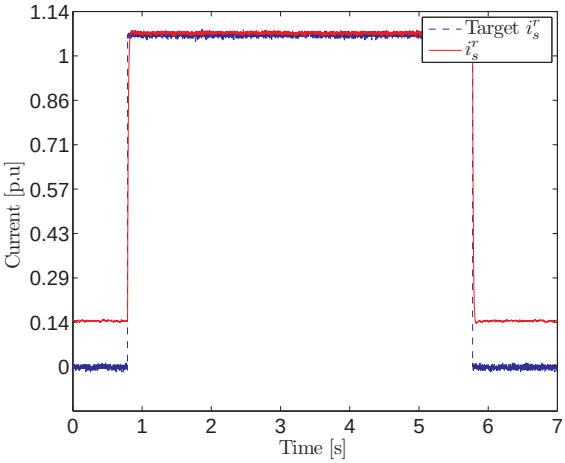

Figure 10: Torque controller applying 1 p.u load to IM

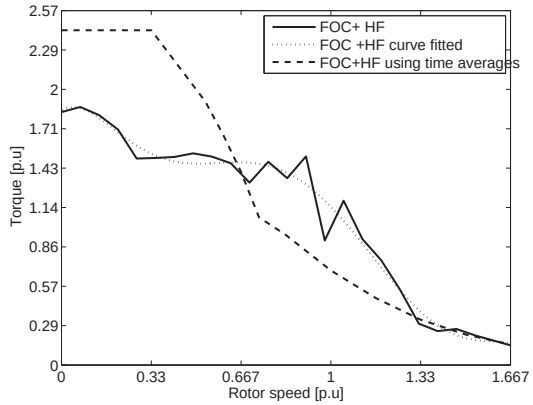

Figure 11: Limits of stable operation

5 Conclusion

In this paper a simplified method of sensorless control through alternating high frequency injection is presented. The proposed method moved away from the conventional method of using a band pass filter in the demodulation scheme. Only the conventional low pass filter is retained during demodulation.

Experimental results show that this method is able to track the position through the entire speed range and beyond base speed under various load conditions. Speed control tests revealed that the performance of the proposed method is comparable to that of "sensored" operation. Tests revealed that the method handles direction changes efficiently. Limits of stable operation tests showed that the method is stable up to almost twice rated torque at standstill in torque control, and able to produce rated torque at rated speed.

The implementation of the proposed method is simple and neglecting the band pass filter reduces the number of parameters that need to be tuned to produce the desired performance. With all the outcome results considered, this method might be suitable as an industrial solution in RSM drive applications.

References

[1] N. Bianchi and S. Bolognani. Influence of Rotor Geometry of an IPM Motor on Sensorless Control Feasibility. *IEEE Transactions on Industry Applications*, 43(1):87–96, 2007.

[2] N. Bianchi, S. Bolognani, J.-H. Jang, and S.-K. Sul. Comparison of PM motor structures and sensorless control techniques for zero-speed rotor position detection. *Power Electronics, IEEE Transactions on*, 22(6):2466 –2475, Nov. 2007.

[3] A. Fratta and A. Vagati. A reluctance motor drive for high dynamic performance application. *IEEE Transactions on Industry Applications*, 28(4):873 –879, Jul/Aug 1992.

[4] W. Hammel and R. Kennel. Position sensorless control of pmsm by synchronous injection and demodulation of alternating carrier voltage. In *Sensorless Control for Electrical Drives (SLED), 2010 First Symposium on*, pages 56 –63, July 2010.

[5] P. Landsmann, D. Paulus, P. Stolze, and R. Kennel. Saliency based encoderless predictive torque control without signal injection for a reluctance synchronous machine. In *Power Electronics and Motion Control Conference (EPE/PEMC), 2010 14th International*, pages S1–10–S1–17, Sept. 2010.

[6] R. Leidhold and P. Mutschler. Improved method for higher dynamics in sensorless position detection. In *Industrial Electronics, 2008. IECON 2008. 34th Annual Conference of IEEE*, pages 1240 –1245, Nov. 2008.

[7] M. Linke, R. Kennel, and J. Holtz. Sensorless speed and position control of synchronous machines using alternating carrier injection. In *Electric Machines and Drives Conference, 2003. IEMDC'03. IEEE International*, volume 2, pages 1211 – 1217 vol.2, June 2003.

[8] J. G. Proakis and D. K. Manolakis. *Digital Signal Processing (4th Edition)*. Prentice Hall, Mar. 2006.

[9] D. Raca, P. Garcia, D. Reigosa, F. Briz, and R. Lorenz. A comparative analysis of pulsating vs. rotating vector carrier signal injection-based sensorless control. In *Applied Power Electronics Conference and Exposition, 2008. APEC 2008. Twenty-Third Annual IEEE*, pages 879 –885, Feb. 2008.

[10] Q. Xin, Z. Xiao-min, W. Chang-song, Z. Li-ping, and W. Hui. Sensorless control of permanent-magnet synchronous motor based on high-frequency signal injection and kalman filter. In *Systems and Control in Aerospace and Astronautics, 2008. ISSCAA 2008. 2nd International Symposium on*, pages 1 –5, Dec. 2008.

[11] H. Zhu, X. Xiao, and Y. Li. A simplified high frequency injection method for PMSM sensorless control. In *Power Electronics and Motion Control Conference, 2009. IPEMC '09. IEEE 6th International*, pages 401 –405, May 2009.